Breaking through the Optimization Limits of Power Factor via Pressure-Decoupled Seebeck Coefficient and Electrical Conductivity

Dianzhen Wang(王殿振)[1†], Muhammad Faizan[2†], Jinming Zhu(朱金铭)[1], Wanting Quan(全婉婷)[1], Yanli Chen(陈延丽)[3], Qiang Zhou(周强)[1], Kuo Bao(包括)[1], Yan Li(李岩)[1], Qiang Tao(陶强)[1*], Lijun Zhang(张立军)[2*], Tian Cui(崔田)[4*], and Pinwen Zhu(朱品文)[1*]

[1]*Synergetic Extreme Condition High-Pressure Science Center, State Key Laboratory of High Pressure and Superhard Materials, College of Physics, Jilin University, Changchun 130012, China*
[2]*School of Materials Science and Engineering, Jilin University, Changchun 130012, China*
[3]*Key Laboratory of Functional Materials Physics and Chemistry of the Ministry of Education, Jilin Normal University, Changchun 130103, China*
[4]*School of Physical Science and Technology, Ningbo University, Ningbo 315211, China*

(Received 11 April 2025; accepted manuscript online 7 May 2025)

In thermoelectricity, the inherent coupling between electrical conductivity and Seebeck coefficient represents a fundamental challenge in thermoelectric materials development. Herein, we present a unique pressure-tuning strategy using compressible layered 2H-$MoTe_2$, achieving an effective decoupling between the electrical conductivity and Seebeck coefficient. The applied pressure simultaneously induces two complementary effects: (1) bandgap reduction that moderately enhances carrier concentration to improve the electrical conductivity, and (2) band convergence that dramatically increases density-of-states effective mass to boost the Seebeck coefficient. This dual mechanism yields an extraordinary 18.5-fold enhancement in the average power factor. First-principles calculations and Boltzmann transport modeling precisely reproduce the experimental observations, validating this pressure-induced decoupling mechanism. The pressure-tuning mechanism provides a feasible and effective strategy for breaking through the optimization limits of the power factor, facilitating the design of high-performance thermoelectric materials.

DOI: 10.1088/0256-307X/42/6/066401 CSTR: 32039.14.0256-307X.42.6.066401

1. Introduction. Thermoelectric (TE) materials have been extensively investigated due to their ability of direct convert heat to electricity without environmental pollution.[1–3] The TE conversion efficiency relies on carrier and phonon transport and is quantified by the dimensionless figure of merit $ZT = S^2\sigma T/\kappa$, where S (Seebeck coefficient), σ (electrical conductivity), and κ (thermal conductivity) are interdependent parameters that pose a fundamental optimization challenge. This complexity mainly arises from the interactions between carriers and phonons. Current strategies like the "phonon-glass electron-crystal" concept partially address this issue by trying to separate the carrier and phonon transport through structural engineering.[4] However, the intrinsic trade-off between S and σ because of the contrasting effects of carrier concentration (n) and density-of-states effective mass (m^*) remains a critical limitation.[5–8] Consequently, identifying effective strategies to decouple S and σ is key to advancing the development of high-performance TE materials.

The interdependence between S and σ is fundamentally governed by the material's band structure characteristics.[9] This coupling can be strategically tuned through manipulating the complexity of the band structure, thereby altering carrier transport.[5] For example, the typical band engineering strategies such as band flattening,[10–12] band degeneracy,[13–15] and introducing resonant levels,[16–18] can result in complex band structures, thereby weakening this coupling relationship. While these methods effectively enhance S via enhancing m^*, a critical trade-off emerges: structural modifications (foreign atoms) from doping or alloying disrupt the lattice periodicity, intensifying the carrier scattering that degrades σ. This inherent conflict between band engineering and lattice integrity preservation highlights the core challenge in achieving true decoupling between S and σ.

In view of this, to ensure the lattice integrity preservation, we turned our attention to the high-pressure effect, which is considered a clean physical modulation without altering the chemical composition.[19] The crystal structure under high pressure facilitates interatomic orbital hybridization and unique lattice strain, which can reduce the bandgap and induce unusual electronic states.[20–23] This offers carrier concentration optimization (for improving σ) and complex band transport characteristics (for enhancing S), which favor the decoupling of S and σ.

†These authors contributed equally to this work.
*Corresponding author. Email: qiangtao@jlu.edu.cn; lijun_zhang@jlu.edu.cn; cuitian@nbu.edu.cn; zhupw@jlu.edu.cn
© 2025 Chinese Physical Society and IOP Publishing Ltd. All rights, including for text and data mining, AI training, and similar technologies, are reserved.

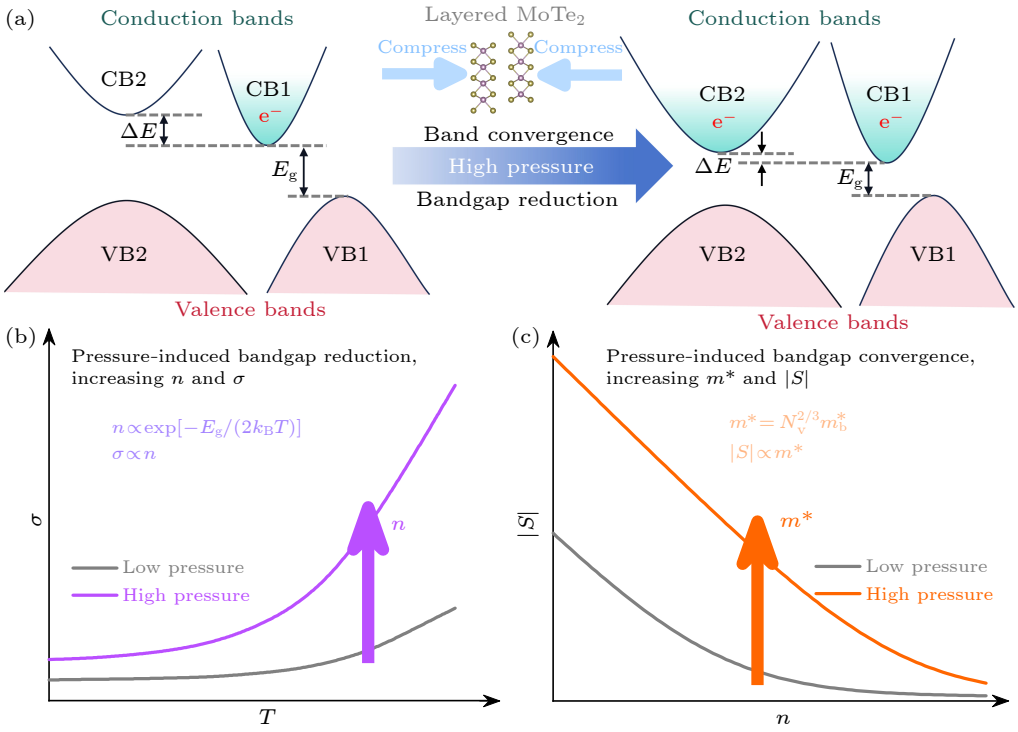

Fig. 1. The mechanism of decoupling $|S|$ and σ via physical pressure. (a) Schematic illustrating the pressure-decoupled $|S|$ and σ; (b) Pressure-induced bandgap reduction increasing n for improving σ; (c) Conduction band convergence increasing N_v for enhancing $|S|$.

Herein, we propose an effective pressure-modulating mechanism for decoupling S and σ in 2H-$MoTe_2$, leveraging its highly compressible layered structure. High pressure enhances the interlayer interaction in 2H-$MoTe_2$, inducing significant band structure modifications that facilitate TE transport tuning. Experimentally, S and σ simultaneously increase with increasing pressure (1–5.5 GPa, 300–1100 K), as confirmed by an in-house technique of *in situ* TE transport properties measurement under high pressure and high temperature (HPHT).[24] Theoretically, first-principles calculations reveal that pressure reduces the bandgap (E_g) while inducing a pronounced conduction band convergence [Fig. 1(a)]. The pressure-reduced E_g favors an increase in n, thereby enhancing σ [Fig. 1(b)]. Meanwhile, the pressure-induced band convergence reduces the energy difference between the neighboring bands (ΔE), increasing the band degeneracy (N_v) and m^*, thereby improving $|S|$ (the absolute value of S) [Fig. 1(c)]. Consequently, a simultaneous improvement of both $|S|$ and σ, i.e., the true decoupling between them is achieved through this pressure-decoupled mechanism.

2. Methods. High-quality bulk precursors for *in situ* HPHT TE transport measurements were prepared via HPHT synthesis combined with spark plasma sintering. Detailed synthesis procedures are provided in the Supplementary Material (SM). The X-ray diffraction (XRD) pattern of $MoTe_2$ in Fig. 2(a) confirms a well-crystallized 2H phase with a typical layered structure. In doped $MoTe_2$, tellurium-rich secondary phases (e.g., $NbTe_4$, Nb_2Te_3, and Nb_5Te_4) were observed [Fig. 2(a)]. These tellurium-rich compounds promote Te vacancy formation,

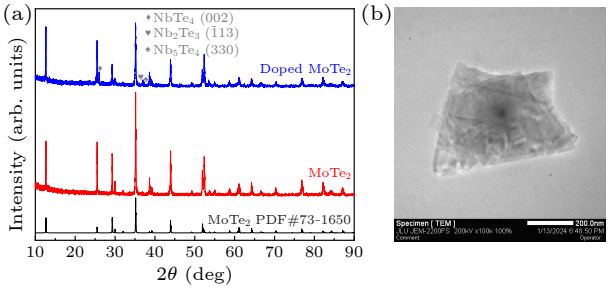

Fig. 2. Structure characterizations. (a) XRD patterns of synthesized $MoTe_2$ and doped $MoTe_2$ through the HPHT method; (b) TEM image of prepared $MoTe_2$ precursor.

providing additional electrons and resulting in N-type semiconductor behavior. Besides, transmission electron microscope (TEM) imaging [Fig. 2(b)] further reveals the nanoflake morphology of 2H-$MoTe_2$, consistent with its layered nature. TE transport properties were investigated using a self-developed *in situ* HPHT measurement system (Fig. S1 in SM). Notably, while the layered structural characteristic implies anisotropic TE behavior, high-quality polycrystalline bulk precursors were employed to minimize anisotropy effects, ensuring macroscopic and homogeneous transport properties.

3. Results and Discussion. The temperature-dependent TE transport properties were investigated under 1–5.5 GPa and 300–1100 K. As pressure increases, both pristine and doped $MoTe_2$ show progressively increasing σ while maintaining semiconducting behavior [Figs. 3(a) and 3(e)]. Besides, it is evident that doped $MoTe_2$ exhibits higher σ due to its higher carrier concentration

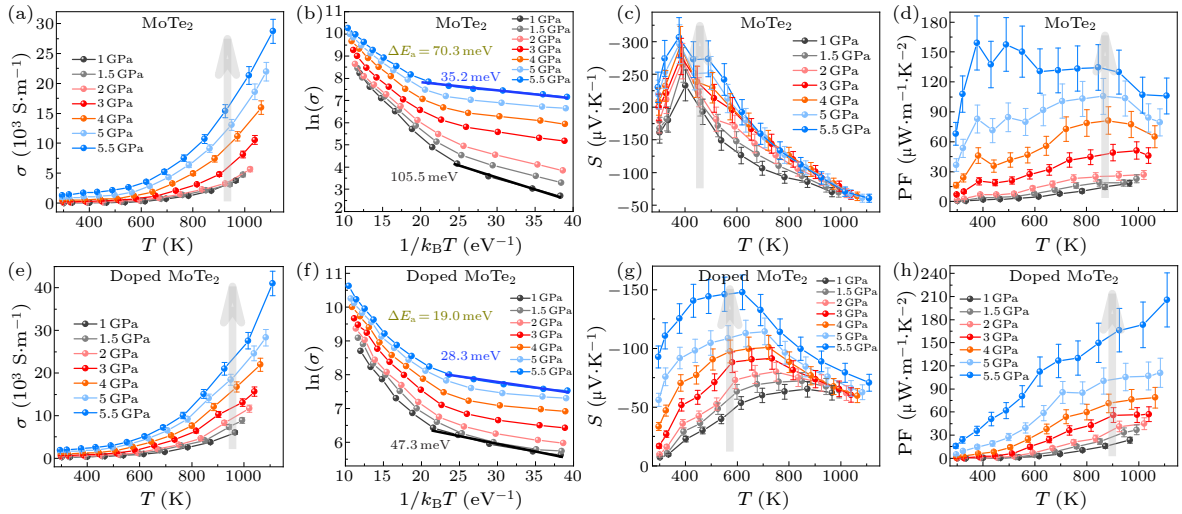

Fig. 3. TE transport properties under HPHT. Temperature-dependent (a), (e) electrical conductivity, (b), (f) Arrhenius plot for linear fit, (c), (g) absolute value of Seebeck coefficient, and (d), (h) power factor of $MoTe_2$ and doped $MoTe_2$ under different pressures.

($\sim 10^{19}\,\mathrm{cm}^{-3}$ vs $\sim 10^{18}\,\mathrm{cm}^{-3}$ for pristine at ambient conditions). Furthermore, the temperature-dependent σ for both $MoTe_2$ and doped $MoTe_2$ shows a typical Arrhenius behavior [Figs. 3(a) and 3(e)], indicating that conduction is dominated by the inter-band transitions above room temperature.[25] To elucidate the σ optimization mechanism under HPHT, we analyzed the semiconducting transport characteristics using the Arrhenius model,[25]

$$\sigma = \sigma_0 \exp\Big(-\frac{E_a}{k_B T}\Big), \tag{1}$$

where σ is a constant, k_B is the Boltzmann constant, and E_a is the activation energy, respectively. With increasing pressure, the activation energy (E_a) of $MoTe_2$ decreases from 105.5 meV (1 GPa) to 35.2 meV (5.5 GPa) [Fig. 3(b)], demonstrating enhanced inter-band transitions for charge transport. This reflects the pressure-induced bandgap reduction, primarily caused by strengthened interlayer interactions.[26] In doped $MoTe_2$, the higher initial carrier concentration caused by doping leads to an initially superior carrier transport property, resulting in systematically lower E_a compared to pristine $MoTe_2$ under equivalent HPHT conditions [Fig. 3(f)].

The negative Seebeck coefficient (S) suggests n-type conduction dominated by electrons. For $MoTe_2$, $|S|$ increases with rising pressure, especially at lower temperatures [Fig. 3(c)]. Typically, the interdependence of TE transport parameters results in a strong coupling between $|S|$ and σ described by[27]

$$|S| = \frac{8\pi^2 \kappa_B^2 T}{3eh^2} m^* \Big(\frac{\pi}{3n}\Big)^{2/3}, \tag{2}$$

$$\sigma = ne\mu, \tag{3}$$

$$\mu \propto 1/m_b^*, \tag{4}$$

$$m^* = N_v^{2/3} m_b^*, \tag{5}$$

where e is the elementary charge, h is the Planck constant, μ is the carrier mobility, N_v is the valley degeneracy, and m_b^* is the effective mass of single band, respectively. The inherent coupling between $|S|$ and σ, mainly arising from their opposing dependencies on n and m^*, has historically constrained the power factor (PF $= S^2\sigma$) optimization. Remarkably, our study reveals simultaneous enhancement in both $|S|$ and σ with increasing pressure across a broad temperature range, leading to synergistic PF improvement [Figs. 3(d) and 3(h)]. Ultimately, at the highest testing pressure of 5.5 GPa, the average PF increases by 18.5-fold for $MoTe_2$ and 18.0-fold for doped $MoTe_2$ compared to the initial testing pressure of 1 GPa. Moreover, the temperature-dependent TE transport properties under ambient pressure (Fig. S2 in SM) show much lower PF values, demonstrating the efficacy of high pressure for enhancing the TE performance. Such a notable enhancement in PF is attributed to the pressure-decoupled $|S|$ and σ for breaking through the optimization limits of PF.

Notably, $|S|$ in $MoTe_2$ decreases above $\sim$400 K [Fig. 3(c)], primarily due to the bipolar effect arising from the small bandgap.[28,29] Specifically, at elevated temperatures, thermally excited minority carriers generate a Seebeck coefficient with the opposite sign, thus degrading the $|S|$. In addition to the pressure-induced reduction of the bandgap to accelerate the bipolar effect, generally, with increasing temperature, the bandgap will be reduced because of the enhanced lattice vibrations and electron–phonon interactions.[30] Hence, under HPHT, the bipolar effect should be effectively suppressed to achieve a higher TE performance.

In doped $MoTe_2$, the addition of electrons significantly weakens the contribution of thermally excited minority holes to S, effectively suppressing the bipolar effect. This aligns with our earlier study about the suppression of the bipolar effect under HPHT.[31] Hence, $|S|$ in doped $MoTe_2$ does not decrease until higher temperatures (above $\sim$600 K) [Fig. 3(g)]. Furthermore, it is evident that the pressure-induced decoupling between $|S|$ and σ becomes

more pronounced when the bipolar effect is minimized. Here, it should be noted that the doped $MoTe_2$ is intentionally designed to suppress the bipolar effect, thereby magnifying the effect of increased $|S|$ with rising pressure, this specific aspect falls outside the scope of our theoretical framework.

To elucidate the decoupling behavior between $|S|$ and σ in $MoTe_2$ under high pressure, we conducted first-principles calculations on the band structure under high pressure. As pressure increases, the bandgap E_g narrows significantly due to enhanced interlayer interactions [Figs. 4(a)–4(d)], leading to an increased carrier concentration and consequently improved σ. Notably, the energy separation between the primary conduction band (CB1, red) at the Σ point and the secondary conduction band (CB2, pink) at the K point decreases from 0.43 eV (0 GPa) to 0.07 eV (7 GPa), demonstrating a pronounced band convergence behavior.[13–15] This pressure-induced convergence effectively transforms the carrier transport from single-band to multi-band behavior, which complicates the carrier transport.

In multi-band transport systems, the density-of-states effective mass m^* is determined by Eq. (5). The Brillouin zone exhibits valley degeneracy N_v of 6 at both K and Σ points according to their geometric symmetry.[13,32] Pressure-induced convergence of CB1 and CB2 doubles N_v to 12, substantially enhancing m^*. Concurrently, this band convergence increases the total density of states near the conduction band minimum with rising pressure [Figs. 4(e)–4(h)], which enhances $|S|$ and thus contributes to the decoupling of $|S|$ and σ in 2H-$MoTe_2$.

To verify the decoupling mechanism attributed to pressure-induced bandgap reduction and band convergence in 2H-$MoTe_2$, we performed TE transport calculations combining first-principles calculations and Boltzmann transport theory.[33,34] The results reveal that σ maintains typical semiconducting behavior under varying pressures [Fig. 4(i)], with increasingly temperature-dependent trends with rising pressure due to the pressure-induced bandgap reduction. Meanwhile, the pressure-induced band convergence enhances m^*, leading to a net increase in $|S|$ with rising pressure, particularly at low temperatures [Fig. 4(j)]. Additionally, in the doped $MoTe_2$, although the main phase of 2H-$MoTe_2$ dominated the TE

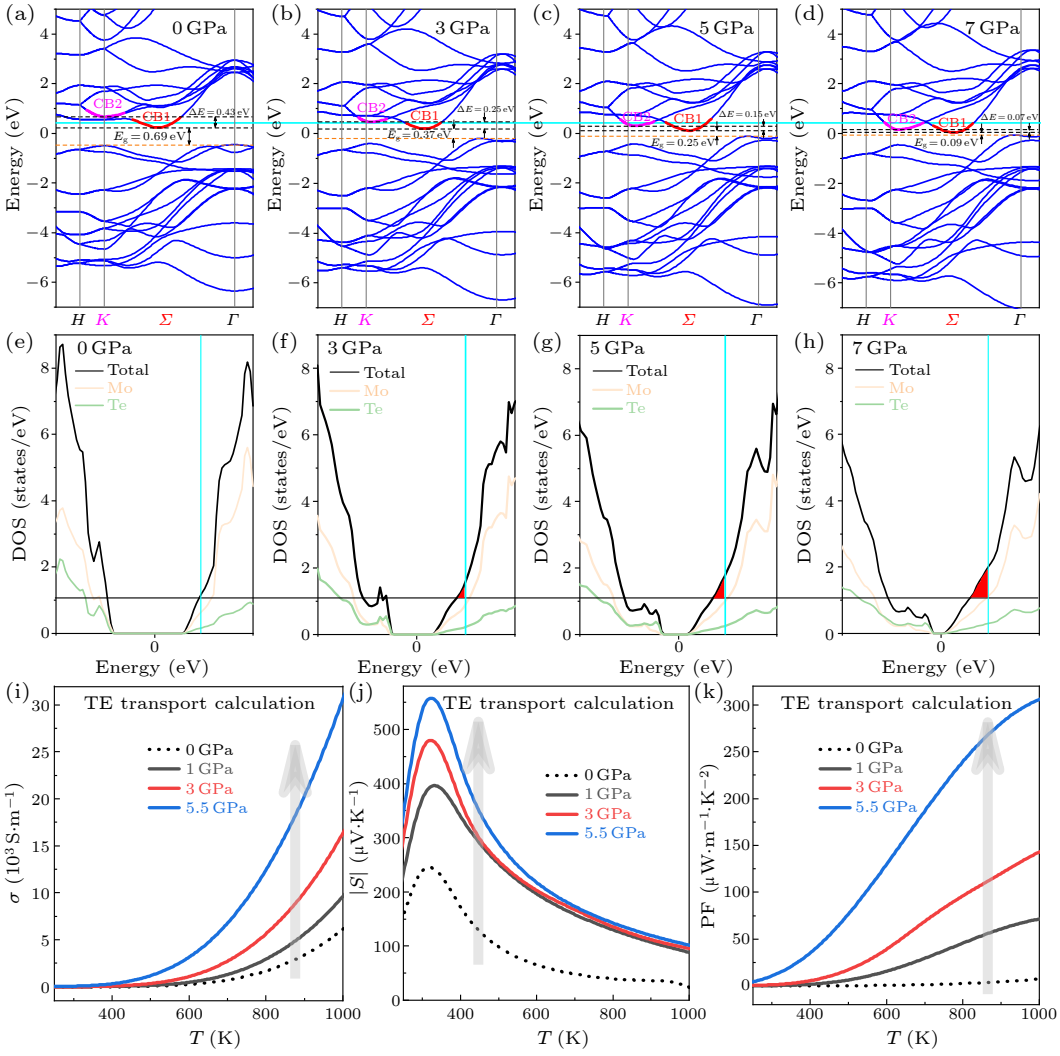

Fig. 4. TE transport calculation of $MoTe_2$ under HPHT. (a)–(d) Calculated band structures and (e)–(h) DOS of $MoTe_2$ under 0 GPa, 3 GPa, 5 GPa, and 7 GPa, respectively. Calculated temperature-dependent (i) σ, (j) $|S|$, and (k) PF of $MoTe_2$ under varying pressures.

transport and the higher carrier concentration suppressed the bipolar effect, resulting in a more pronounced decoupling behavior between $|S|$ and σ, it should be noted that the formed heterointerface between the $MoTe_2$ phase and these tellurium-rich compounds might cause a carrier energy filtering effect,[1] thus contributing to the enhancement of the Seebeck coefficient with increasing pressure. As a result, the pressure-induced decoupling of $|S|$ and σ breaks through the optimization limits of PF, enabling significant PF enhancement under HPHT [Fig. 4(k)].

To further elucidate the respective contributions of pressure-induced bandgap reduction and band convergence to decoupling between $|S|$ and σ, we performed high-pressure Hall effect measurements (see the SM for experimental details). Figure 5(a) shows the pressure dependence of carrier concentration n and mobility μ in 2H-$MoTe_2$. The observed moderate increase in n with rising pressure follows the expected trend $n \propto \exp(-E_g/2k_BT)$, consistent with the pressure-induced bandgap reduction. Meanwhile, μ decreases due to enhanced intervalley scattering.[13,35] Therefore, the net increase in σ is primarily driven by the increasing n.

To quantitatively evaluate the enlarged m^*, we simulated $|S|$ as a function of n using a restructured single parabolic band model,[36] The Pisarenko plots in Fig. 5(b) reveal a substantial increase in m^* with rising pressure. Quantitative analysis at three representative pressures shows m^* increasing progressively from $0.2\,m_e$ (m_1^*, 1 GPa) to $0.5\,m_e$ (m_3^*, 3 GPa), then to $1.2\,m_e$ ($m_{5.5}^*$, 5.5 GPa).

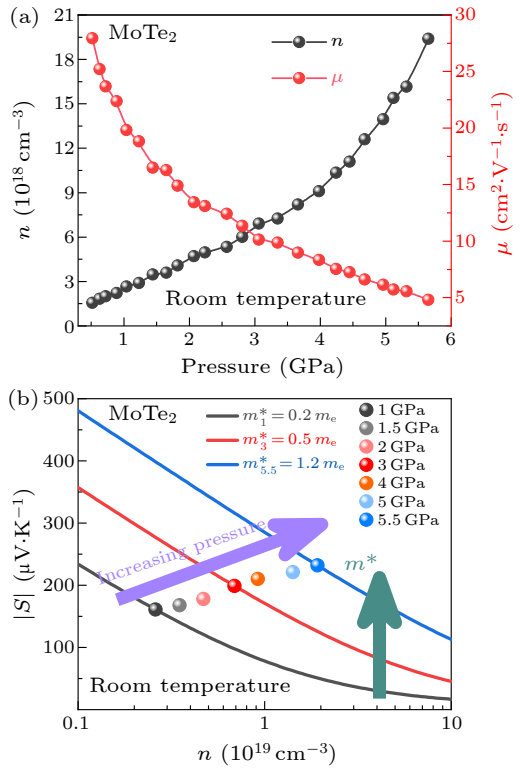

Fig. 5. Carrier transport properties under high pressures. (a) Measured carrier concentration and mobility, and (b) room-temperature Pisarenko plots of $MoTe_2$ under varying pressures.

Such a notable enhancement in m^* under high pressure clearly demonstrates the impact of pressure-induced band convergence, which compensates for the negative contribution of the increased n to $|S|$, ultimately resulting in the simultaneous optimization of both $|S|$ and σ.

It was reported that pressure-induced electronic topological transition (ETT) significantly enhanced the carrier mobility μ by inducing new metallic Fermi surface states.[37,38] However, this increase in μ was typically accompanied by a substantial increase in n, which tended to compromise $|S|$.[37,38] In contrast, 2H-$MoTe_2$ exhibits only a moderate increase in n due to the gradual reduction in bandgap with increasing pressure. This restrained increase in n permits the dramatic enhancement in m^* caused by the pressure-induced band convergence to dominate, yielding a net increase in $|S|$ while maintaining an increase in σ. Thus, unlike the pressure-induced ETT, our observed simultaneous bandgap reduction and band convergence under high pressures represent a unique mechanism for genuine decoupling between $|S|$ and σ, offering distinct advantages for TE optimization.

While Qin *et al.* reported a strategy to achieve the simultaneous optimization of μ and m^* in SnSe through valence band alignment, thereby achieving a simultaneous optimization in S and σ in the SnSe crystal.[39] However, the n was observed to decrease as a result of the increased bandgap caused by the alloying process, which makes σ seem not to increase much, especially at high temperatures. Furthermore, alloying-induced carrier scattering restricted further improvements in μ and σ. It should be noted that μ is highly sensitive to extrinsic factors like grain boundaries and defects,[5] implying that such band engineering benefits are only fully realized in extremely high purity or even single crystals. In contrast, our pressure-driven approach in layered $MoTe_2$ simultaneously enhances both n (through bandgap reduction) and m^* (via band convergence). This provides a more direct and efficient route for TE transport optimization, as increasing n offers inherent advantages for improving σ in most cases. The pressure-tuning method thus presents a more universally applicable approach for optimizing TE transport properties.

4. Conclusion. In summary, we demonstrate a novel pressure-induced decoupling mechanism between the Seebeck coefficient and electrical conductivity in layered 2H-$MoTe_2$ through combined high-pressure experiments and theoretical analysis. First-principles calculations coupled with Boltzmann transport theory reveal that simultaneous pressure-induced bandgap reduction and band convergence produce two complementary effects: (1) moderate enhancement of carrier concentration through bandgap reduction, and (2) significant increase in density-of-states effective mass via band convergence. These effects were quantitatively verified through high-pressure Hall measurements and band transport modeling. The synergistic function of these mechanisms enables a remarkable 18.5-fold enhancement of the average power factor in 2H-$MoTe_2$. Our findings establish high-pressure tuning as a

powerful strategy for breaking through the optimization limits of the power factor, providing constructive insights for the design of high-performance TE materials. See the SM for the experimental and theoretical calculation details. The self-developed schematic diagram of *in situ* thermoelectric transport properties measurement under HPHT and TE transport properties under ambient pressure of $MoTe_2$ and doped $MoTe_2$ is also shown in the SM.

Acknowledgments. This work was supported by the Science and Technology Development Project of Jilin Province (Grant No. SKL202402004), the Program for the Development of Science and Technology of Jilin Province (Grant No. YDZJ202201ZYTS308), the Open Research Fund of State Key Laboratory of Inorganic Synthesis and Preparative Chemistry, Jilin University (Grant Nos. 2022-16 and 2022-23), and the National Natural Science Foundation of China (Grant No. 12350410372). The authors acknowledge "Solid Environment High Pressure and High Temperature (SEHPHT) Station" for all of high pressure experiments.

References

[1] Wang D, Gao Y, You C, Cheng J, Liu Z, Qiang Y, Lian M, Ma X, Ge Y, Chen Y, Tao Q, and Zhu P 2024 *Adv. Funct. Mater.* **34** 2308970
[2] Beretta D, Neophytou N, Hodges J M, Kanatzidis M G, Narducci D, MartinGonzalez M, Beekman M, Balke B, Cerretti G, Tremel W, Zevalkink A, Hofmann A I, Müller C, Dörling B, Campoy-Quiles M, and Caironi M 2019 *Mater. Sci. Eng. R Reports* **138** 100501
[3] Jiang B, Yu Y, Cui J, Liu X, Xie L, Liao J, Zhang Q, Huang Y, Ning S, Jia B, Zhu B, Bai S, Chen L, Pennycook S J, and He J 2021 *Science* **371** 830
[4] Snyder G J, Christensen M, Nishibori E, Caillat T, and Iversen B B 2004 *Nat. Mater.* **3** 458
[5] Xiao C, Li Z, Li K, Huang P C, and Xie Y 2014 *Acc. Chem. Res.* **47** 1287
[6] Shi X, Chen W, Tao X, Zou J, and Chen Z 2020 *Mater. Horiz.* **7** 3065
[7] Zhang G and Zhang Y 2017 *J. Mater. Chem. C* **5** 7684
[8] Shi X, Tao X, Zou J, and Chen Z 2020 *Adv. Sci.* **7** 1902923
[9] Yang J, Xi L, Qiu W, Wu L, Shi X, Chen L, Yang J, Zhang W, Uher C, and Singh D J 2016 *NPJ Comput. Mater.* **2** 15015
[10] Dutta M, Biswas R K, Pati S K, and Biswas K 2021 *ACS Energy Lett.* **6** 1625
[11] Wang H, Hu H, Man N, Xiong C, Xiao Y, Tan X, Liu G, and Jiang J 2021 *Mater. Today Phys.* **16** 100298
[12] Li J, Zhang X, Ma H, Duan B, Li G, Yang J, Wang H, Yang H, Zhou L, and Zhai P 2022 *J. Materiomics* **8** 88
[13] Pei Y, Shi X, LaLonde A, Wang H, Chen L, and Snyder G 2011 *Nature* **473** 66
[14] Tan G, Shi F, Hao S, Zhao L, Chi H, Zhang X, Uher C, Wolverton C, Dravid V P, and Kanatzidis M G 2016 *Nat. Commun.* **7** 12167
[15] Huang X, Li J, Ma H, Li C, Liu T, Duan B, Zhai P, and Li G 2024 *Chin. Phys. Lett.* **41** 077102
[16] Heremans J P, Wiendlocha B, and Chamoire A M 2012 *Energy Environ. Sci.* **5** 5510
[17] Tan G, Shi F, Hao S, Chi H, Zhao L, Uher C, Wolverton C, Dravid V P, and Kanatzidis M G 2015 *J. Am. Chem. Soc.* **137** 5100
[18] Zhang Q, Liao B, Lan Y, Lukas K, Liu W, Esfarjani K, Opeil C, Broido D, Chen G, and Ren Z 2013 *Proc. Natl. Acad. Sci.* **110** 13261
[19] Morozova N V, Korobeinikov I V, and Ovsyannikov S V 2019 *J. Appl. Phys.* **125** 220901
[20] Badding J V 1998 *Annu. Rev. Mater. Sci.* **28** 631
[21] Li Y, Liu J, Wu B, Tao Y, Geng Y, Wang X, and Lei L 2024 *Chin. Phys. Lett.* **41** 047803
[22] Zheng B, Chen T, Sun H, Yang M, Yang B, Chen X, Zhang Y, and Liu X 2024 *Chin. Phys. Lett.* **41** 057301
[23] Zhang L, Wang Y, Lv J, and Ma Y 2017 *Nat. Rev. Mater.* **2** 17005
[24] Zhao W, Cheng J, Wang D, You C, Zhang J, Ye M, Wang X, Dong S, Tao Q, and Zhu P 2022 *Rev. Sci. Instrum.* **93** 103901
[25] Cutler M and Mott N F 1969 *Phys. Rev.* **181** 1336
[26] Berri S and Bouarissa N 2021 *Comput. Condens. Matter* **28** e00574
[27] Lee D S, An T, Jeong M, Choi H S, Lim Y S, Seo W S, Park C H, Park C, and Park H H 2013 *Appl. Phys. Lett.* **103** 232110
[28] Gong J, Hong A, Shuai J, Li L, Yan Z, Ren Z, and Liu J 2016 *Phys. Chem. Chem. Phys.* **18** 16566
[29] Guo Z, Song K, Yan Z, Sun P, Tan X, Wu G, Zhang Q, Liu G, Yu B, and Jiang J 2021 *Chem. Eng. J.* **426** 131853
[30] Geng P, Li W, Zhang X, Zhang X, Deng Y, and Kou H 2017 *J. Phys. D: Appl. Phys.* **50** 40LT02
[31] Wang D, You C, Ge Y, Wang F, Wang X, Liang X, Zhou Q, Tao Q, Chen Y, and Zhu P 2024 *Appl. Phys. Lett.* **125** 013903
[32] Zhang C, Li Z, Zhang M, Xie H, Li X, Su X, Yan Y, Chi H, Uher C, Liu W, and Tang X 2019 *ACS Appl. Mater. Interfaces* **11** 26069
[33] Kresse G and Furthüller J 1996 *Comput. Mater. Sci.* **6** 15
[34] Madsen G K H, Carrete J, and Verstraete M J 2018 *Comput. Phys. Commun.* **231** 140
[35] Park J, Dylla M, Xia Y, Wood M, Snyder G J, and Jain A 2021 *Nat. Commun.* **12** 3425
[36] Zhu J, Zhang X, Guo M, Li J, Hu J, Cai S, Cai W, Zhang Y, and Sui J 2021 *Npj Comput. Mater.* **7** 116
[37] Chen L, Chen P, Li W, Zhang Q, Struzhkin V V, Goncharov A F, Ren Z, and Chen X. 2019 *Nat. Mater.* **18** 1321
[38] Bai F, Yu H, Peng Y, Li S, Yin L, Huang G, Chen L, Goncharov A F, Sui J, Cao F, Mao J, Zhang Q, and Chen X 2022 *Adv. Sci.* **9** 2105709
[39] Qin B, Wang D, Liu X, Qin Y, Dong J, Luo J, Li J W, Liu W, Tan G, Tang X, Li J, He J, and Zhao L 2021 *Science* **373** 556